

5th US Combustion Meeting
Organized by the Western States Section of the Combustion Institute
and Hosted by the University of California at San Diego
March 25-28, 2007.

Theory of Bouncing and Coalescence in Droplet Collision

P. Zhang and C. K. Law

Department of Mechanical and Aerospace Engineering

Princeton University, Princeton, New Jersey 08544

Droplet collision, coalescence, and bouncing are frequent events in dense sprays. A comprehensive theory was formulated to describe the dynamics of these processes for the head-on collision of two identical droplets. Specific interest was placed on predicting the coalescence and bouncing responses, including descriptions of the droplet deformation, the viscous loss through droplet internal motion, the dynamics and rarefied nature of the gas film between the colliding droplets, and the destruction and thereby merging of the colliding interfaces due to the van der Waals attractive force. The theoretical results agree well with previous experimental observations. Specifically, it is theoretically confirmed that as the impact inertial increases, collision of alkane droplets at one atmospheric pressure results in merging, bouncing and merging again, with the predicted merging Weber numbers agreeing well with the experimental data. Furthermore, the effects of ambient pressure and the rheological properties of the liquid were investigated. It is shown that while bouncing is absent for water droplets at atmospheric pressure, it occurs at higher pressures. Similarly, while bouncing is observed for alkane droplets at atmospheric pressure, it is absent at lower pressures.

1. Introduction

Droplet collision is a frequent event in many natural and industrial processes. A prominent example is the vaporization and combustion of dense sprays in which the high concentration of droplets implies the possibility of droplet collision. It is obvious that the outcome of the collision, in terms of coalescence and bouncing, can substantially influence the subsequent development of the spray characteristics.

Earlier experimental studies were focused on water droplets in atmospheric air [1, 2, 3]. These studies were subsequently extended by Jiang, Umemura & Law [4] and Qian & Law [5] to hydrocarbon droplets in environments that may not be atmospheric air, yielding a unified description of the collision outcome. Specifically, distinct regimes were identified and indicated by the collision Weber number We , which represents the ratio of the inertial force to the surface tension, and an impact parameter, which is a measure of the deviation of the droplet trajectory from that of head-on collision. In the limit of head-on collision between two identical droplets, four regimes of the collision outcome were observed with progressively increasing We from a small value, namely: (I) coalescence, (II) bouncing, (III) coalescence again, and (IV) coalescence followed by separation with the concomitant production of additional daughter droplets. Furthermore, the boundaries between the collision regimes can be significantly influenced by the conditions of the ambient gas and the rheological properties of the droplets. For example, increasing pressure promotes bouncing while increasing surface tension promotes coalescence.

Consequently, while bouncing was absent for water droplets at one atmosphere pressure, it was observed at higher pressures. Similarly, while bouncing was observed for alkane droplets at atmospheric pressure, it was absent at lower pressures.

It is of obvious fundamental and practical interest to be able to theoretically predict the transition boundaries between the different regimes of collision outcomes. Consequently, Qian & Law [5] successfully analyzed the transition from regimes (III) to (IV) as the boundary across which the total energy of the merged mass cannot be contained by its surface energy at maximum deformation. For situations of higher inertia (Regime IV), Roisman [6] proposed a theoretical model with emphasis on the description of the drop breakup associated with the binary collision phenomena. Using asymptotic theory, Gopinath and Koch [7] and Bach, Koch and Gopinath [8] studied the collision between two weakly deformable droplets with We up to unity, focusing on the transition between regimes I and II.

The most challenging aspect of the problem, namely a unified description for the transitions from regimes (I) to (II), and from regimes (II) to (III), has however not been attempted. The objective of the present study is therefore to provide such a formulation. The task is a challenging one because of the nonmonotonic nature of the two transition boundaries with respect to We , of the large deformation of the droplets, of the need to describe the experimental observations of the presence/absence of regime (II) for different collision situations, and of other features that will become evident as the formulation develops.

In the next section we shall present a phenomenological description of the problem of interest, and consequently identify the various factors and hence component processes that need to be analyzed. Formulation of these component processes will then be described in the succeeding sections, which are followed by the calculated results and comparison with the experimental observations.

2. Phenomenology

As the two droplets approach each other, their shape deform from spherical because of the pressure build-up in the intervening gas. The kinetic energy of the droplets is partly converted into their surface energy and partly stored or dissipated through the internal motion within the droplets and the intervening gas. The occurrence of coalescence depends on whether the clearance between two droplets can reach a critical value, at which the molecular attractive force between the two interfaces becomes effective, before the droplets have totally lost the kinetic energy associated with their forward motion. If the impacting interfaces can indeed reach the dimension of molecular interaction, typically a few hundred Angstrom [9], then the attractive van der Waals force gradually dominates over other forces and eventually pulls the two interfaces together. However, when the minimum clearance between the interfaces is larger than this characteristic distance, the droplets will retract under surface tension and consequently bounce away from each other. The receding droplets will accelerate and regain their spherical shape as the surface energy is converted back to their kinetic energy. The droplets however will not be able to regain their original velocity because of viscous dissipation. The collision is therefore inelastic.

Increasing the collision inertia and hence We not only leads to an increase in the pressure of the intervening gas, but it also flattens the interfaces. This flattening increased the surface area in the interfacial gap and hence also tends to prevent coalescence because of the increased resistance

force acting on the droplets. At the same time, however, the outwardly spreading interface drags the intervening gas with them and as such tends to reduce the pressure built-up instead. It is therefore reasonable to expect that the response between coalescence and bouncing with increasing We could be non-monotonic.

Substances with strong intermolecular forces usually have large values of surface tension. Water is among them. This implies that the colliding water droplets may coalesce at larger clearances because of the relatively larger intermolecular force range. This is the underlying reason for the absence of bouncing in water droplet collision at one atmosphere. However, by decreasing the ambient pressure, the intervening gas becomes easier to be squeezed out and merging is promoted. Accordingly, the bouncing regime of water droplet collision is found at higher ambient pressures than that for the hydrocarbons.

The final element of importance in the formulation is that since the colliding interfaces have to reach the dimension of the molecular force, the motion of the gas within the interfacial gap, at and prior to the incipient state of coalescence, must necessarily be that of the rarefied flow. Consequently the interfacial flow spans the entire flow regime, from continuum mechanics to rarefied flows.

Summarizing, description of the collision dynamics must involve the inertia of the droplet motion, the interchange of the kinetic and surface energies as the droplets undergo substantial deformation, the viscous dissipation of the droplet internal motion, the dynamics and rarefied nature of the gaseous film between the colliding interfaces, and the molecular attraction that leads to the destruction and thereby merging of the interfaces.

The formulation to be presented next therefore consists of the following components. We shall first establish a model, in Section 3, to describe the collision dynamics based on conservation laws. The internal motion of droplets and the intervening gas flow are then studied in Sections 4 and 5. These lead to an initial value problem of a system of coupled nonlinear ordinary differential equations that govern the time-dependent variables describing collision dynamics, to be discussed in Section 6. The predictions of the theory and coalescence-bouncing-coalescence transitions are then compared with the experimental results in Section 7, accounting for the effects of ambient pressure and the droplet material.

3. Droplet Dynamics

An obvious difficulty to describe droplet collision with large impact inertia is the need to take into account the possible large deformation. Figure 3.1 shows the schematic of the droplet configuration analyzed. Here the colliding droplet of radius $R(t)$ is assumed to have a flattened disc-shaped interface of radius $a(t)$, which continuously changes as the droplets first approach each other and then retract if merging is not effected. The perpendicular distance from the drop center to the flattened surface is denoted by another time-dependent variable $b(t)$. The droplet initially has radius R_0 and impact velocity V_0 . The droplet is characterized by its density ρ_l , viscosity μ_l , and surface tension σ . The surrounding gas has density ρ_g , viscosity μ_g , and pressure p_0 .

The geometric relation between a , b and R is

$$a^2 + b^2 = R^2 \quad (1)$$

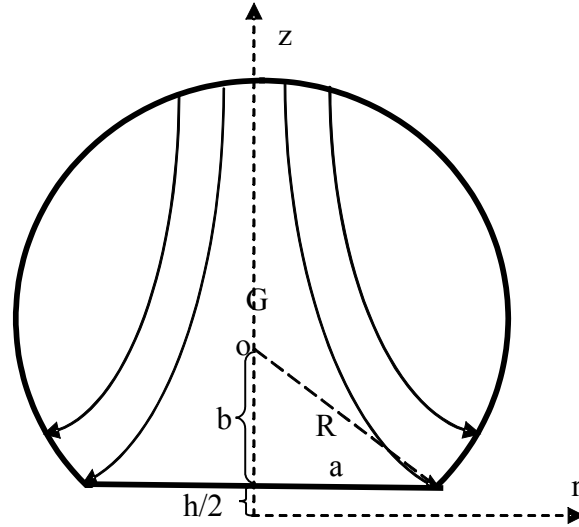


Figure 3.1 Schematic of the droplet configuration

Overall mass conservation for the droplet leads to

$$M = \frac{\pi}{3} \rho_l (2R^3 + 3R^2b - b^3) = M_0 = \frac{4\pi}{3} \rho_l R_0^3 \quad (2)$$

The Newton's equation of motion for the entire droplet is given by

$$\frac{d^2}{dt^2} \left(G + \frac{h}{2} \right) = \frac{F}{M} \quad (3)$$

where G is the distance from the mass center of the droplet to the flattened surface, and h is the gap clearance. G can be expressed in terms of R and b by the following geometric relation

$$G = \frac{3(R-b)^2}{4(2R-b)} + b \quad (4)$$

and in general does not coincide with b . We assume that the axial force acting on the bottom surface is due to the pressure of the intervening gas between the two droplets,

$$F = \int_0^a p(r, z, t) 2\pi r dr \quad (5)$$

The energy budget of the droplet consists of a balance between the changes in its kinetic and surface energies with the viscous dissipation through its internal motion and the work done by the gas, while the viscous loss in the gas phase has been shown to be negligible [5, 10, 11],

$$-\frac{dE_t}{dt} + \frac{dW}{dt} = \frac{d\Sigma}{dt} + \Phi_l \quad (6)$$

The translational energy of the droplet is given by

$$E_t = \frac{1}{2}MV^2 = \frac{1}{2}M \left[\frac{d}{dt}(G + h/2) \right]^2 \quad (7)$$

The work done by the intervening gas per unit time is,

$$\frac{dW}{dt} = F \frac{d(h/2)}{dt} \quad (8)$$

The total surface energy is given by the product of the surface tension, σ , and the total surface area of the droplet,

$$\Sigma = \sigma\pi(3R^2 + 2Rb - b^2) \quad (9)$$

The viscous dissipation of the internal flow is expressed by [12]

$$\Phi_t = \int_0^{R+b} \int_0^{\sqrt{R^2-(z-b)^2}} 2\mu_t \left[\left(\frac{\partial v_r}{\partial r} \right)^2 + \left(\frac{\partial v_z}{\partial z} \right)^2 \right] 2\pi r dr dz \quad (10)$$

Thus, once the internal motion of the droplet and the intervening gas flow are known, the four unknowns, a , b , R and the gap width h can be determined from the above system of equations.

Assuming that the intervening gas pressure can be closely approximated by the droplet internal pressure during the process of the flattening of the droplet, Bradley and Stow [13] analyzed the droplet deformation. While they did not explicitly consider the energy budget, the calculated radius at maximum deformation was in good agreement with the numerical simulation.

4. Droplet Internal Motion

Experimental observations [5] and numerical simulations [10] showed that the droplet deformation is caused by the formation of a straining flow within the droplet characterized by the flattened disc-shaped interface that is also radially spreading outward. In general, the axial velocity of the bottom surface does not coincide with the transitional velocity of the gravity center. This velocity difference results in a strong straining internal motion and the subsequent deformation of the droplet. Furthermore, the internal motion also results in substantial viscous loss, which is a crucial factor in the energy balance. It was shown in [4] that the cumulative viscous dissipation at the maximum deformation can even reach half of the initial kinetic energy of the droplet. Thus an accurate description of the internal motion is essential in the formulation.

A plausible description of the internal motion is a purely straining flow, in which the radial and velocities are respectively $u = \kappa r$ and $w = -2\kappa z$, where κ is the straining rate defined as the rate with which the radius of the flattened disk increases. We have however found that, in the beginning of the droplet deformation, the straining rate κ is very large so that viscous dissipation based on the purely straining flow is substantially overestimated. Actually, in high straining rate situations, the axial momentum transport due to viscosity is suppressed by the induced high-speed axial flow to a very thin region, beyond which the effect of viscosity can be neglected.

We have subsequently recognized that the present problem bears similarity to that of the classical von Kármán's rotating disk [14], in which a flat disk rotates about an axis perpendicular to its

plane with a uniform angular velocity in a stationary fluid. The fluid near the disk is carried by friction and thrown outwardly by the centrifugal force. An induced flow approaches the disk and confines the axial viscous transport to a very thin layer. A self-similar solution exists for a disk of infinite extent because of the lack of a characteristic dimension. This solution has also been found to be a good approximation for a disk of finite radius over a large fraction of the radial direction (up to 90% of the disk radius) when the rotational velocity is sufficiently high [15]. Recognizing the physical similarity between these two problems, in the presence of the tangential velocity of the stagnation surface and its role in inducing the stagnation flow, we seek an analytical solution for the present problem following the same procedure as that of the rotating disk.

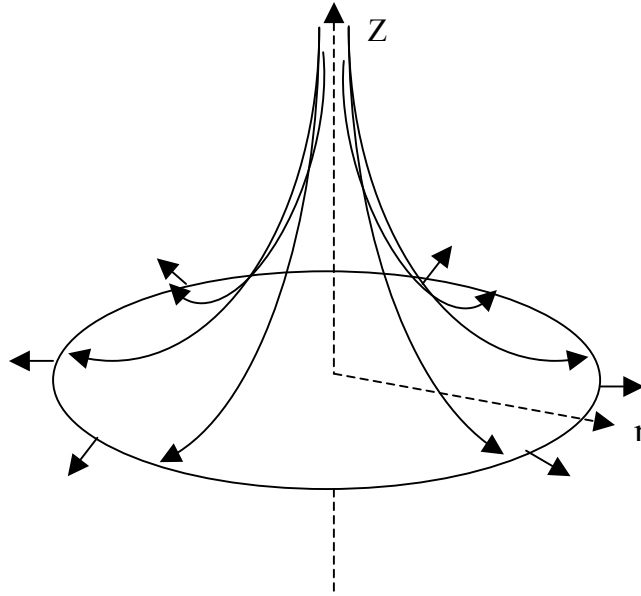


Figure 4.1 Schematic of the induced flow by an expanding disk

Our problem is thus posed as follows (Figure 4.1): an infinite disk, located at the $z = 0$ plane, is immersed in a stagnant fluid. The disk expands outwardly in its plane with a radial velocity $u = \kappa r$, where κ is a specified strain rate. A cylindrical coordinate system (r, ϕ, z) is established on the disk, with the corresponding velocity components denoted by (u, v, w) . We are interested in the steady rotationally motionless ($v \equiv 0$) velocity field of an axisymmetric incompressible flow, that is, in the upper half space, $z > 0$.

The Navier-Stokes equations for such a flow are,

$$u \frac{\partial u}{\partial r} + w \frac{\partial u}{\partial z} = -\frac{1}{\rho} \frac{\partial p}{\partial r} + \nu \left(\frac{\partial^2 u}{\partial r^2} + \frac{1}{r} \frac{\partial u}{\partial r} + \frac{\partial^2 u}{\partial z^2} - \frac{u}{r^2} \right) \quad (11)$$

$$u \frac{\partial w}{\partial r} + w \frac{\partial w}{\partial z} = -\frac{1}{\rho} \frac{\partial p}{\partial z} + \nu \left(\frac{\partial^2 w}{\partial r^2} + \frac{1}{r} \frac{\partial w}{\partial r} + \frac{\partial^2 w}{\partial z^2} \right) \quad (12)$$

and the continuity equation is,

$$\frac{1}{r} \frac{\partial(ru)}{\partial r} + \frac{\partial w}{\partial z} = 0 \quad (13)$$

The no-slip boundary condition at the wall yields:

$$z = 0: \quad u = \kappa r, \quad w = 0 \quad (14)$$

The boundary condition at infinity is given by

$$z = \infty: \quad u = 0 \quad (15)$$

It is noted that, although the flow does not have rotational and radial motion at infinity, there is a finite induced axial velocity.

We assume a similarity solution of the form

$$u = -\frac{r}{2} \frac{df(z)}{dz}, \quad w = f(z), \quad p = p(z) \quad (16)$$

that satisfies the continuity equation. Substituting (16) into (11) and (12), we obtain, respectively

$$\nu f''' - ff'' + \frac{1}{2}(f')^2 = 0 \quad (17)$$

$$\frac{p}{\rho} = -\frac{1}{2}f^2 + \nu f' + const \quad (18)$$

where the superscript ‘’ denotes a derivative with respect to z .

By introducing the transformation

$$z = \sqrt{\nu/\kappa} \zeta, \quad f = \sqrt{\nu\kappa} F \quad (19)$$

where $(\nu/\kappa)^{1/2}$ and $(\nu\kappa)^{1/2}$ are respectively the characteristic length and velocity in the present problem, we can rewrite (17) and the boundary conditions (14) and (15) in nondimensional form as

$$F''' - FF'' + \frac{1}{2}F'^2 = 0 \quad (20)$$

$$\zeta = 0: F = 0, F' = -2; \quad \zeta = \infty: F' = 0 \quad (21)$$

where the superscript ‘’ denotes a derivative with respect to ζ .

Equation (20) has been solved by using three methods, namely the Pohlhausen’s method, series expansion, and numerical integration. These solutions are given below and compared.

Following the classical Pohlhausen’s approach [14] by approximating the radial velocity profile by a fourth-order polynomial, with boundary layer thickness ζ_0 , the radial velocity is found to be

$$F'(\zeta) = \left(\frac{\zeta}{\zeta_0} - 1 \right)^3 \left[\left(2 - \frac{\zeta_0^2}{3} \right) \frac{\zeta}{\zeta_0} + 2 \right] \quad (22)$$

where $\zeta_0 = 3.464$. Integrating the above, with the boundary condition at infinity, readily yields the function F , which represents the axial velocity:

$$F(\zeta) = -\frac{2}{5} \zeta_0 \left[1 + \left(\frac{\zeta}{\zeta_0} - 1 \right)^5 \right] \quad (23)$$

It is seen that the axial velocity has a finite value at infinity, which is a natural result due to continuity.

In using series expansion [16, 17], the governing equation is solved as a power series near $\zeta = 0$ and an asymptotic series for large values of ζ . These two series solutions are then matched at a suitable ζ . Specifically, the power series solution for small ζ that satisfies the governing equation and the boundary conditions at $\zeta = 0$, is

$$F = -2\zeta + A\zeta^2 - \frac{1}{3}\zeta^3 + \frac{1}{30}\zeta^5 - \frac{A}{360}\zeta^6 + \dots \quad (24)$$

where A is a constant to be determined.

Letting $\zeta \rightarrow \infty$, $F' \rightarrow 0$, the solution shows an exponential-like behavior, which implies the existence of a solution in the form of exponential series. The formal expansion that satisfies the equation and the boundary condition at infinity is given by

$$F = -B + Ce^{-B\zeta} - \frac{C^2}{8B}e^{-2B\zeta} + \frac{C^3}{48B^2}e^{-3B\zeta} + \dots \quad (25)$$

where B and C are constants to be determined.

The solutions are matched at a point that F , F' and F'' are all continuous. The three restrictions on F determine the three unknowns constant A , B and C , given by

$$A = 1.202, \quad B = 1.503, \quad C = 1.632 \quad (26)$$

with the matching point located at $\zeta = 0.5991$.

The above solutions are shown in Figure 4.2, together with the numerical solution. The series solution shows very close agreement with the numerical solution while the Pohlhausen's solution has a 10% error in terms of the axial velocity at infinity. Further realizing that the first two terms in (25) actually give a very good approximation to the solution of equation (20) except it does not satisfy the boundary condition at $\zeta = 0$, and that the matching point is very close to $\zeta = 0$, we have forced (25) to satisfy the boundary condition at $\zeta = 0$ and obtained an approximate series solution as:

$$F = -1.503(1 - e^{-1.503\zeta}) \quad (27)$$

that satisfies the boundary conditions both at the wall and infinity. It is seen that this truncated solution agrees well with the numerical solution.

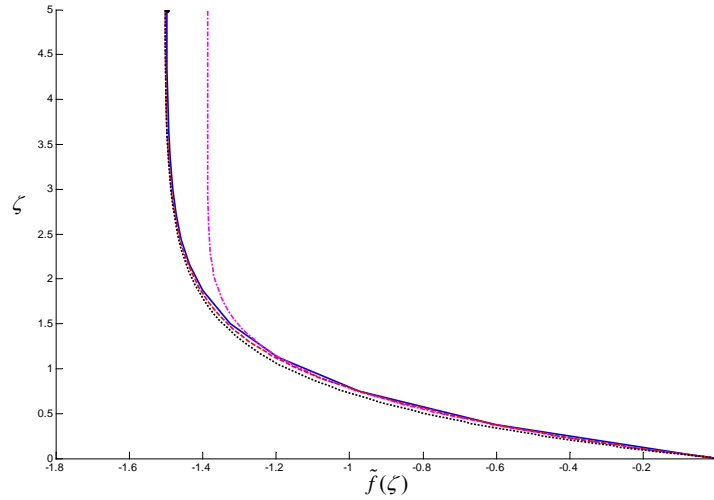


Figure 4.2 Comparison of the three solutions for the droplet internal motion: the Polhausen solution (in purple), the series solution (in red), the numerical solution (in blue), and the approximate solution (in black).

By using the approximate, simple, solution (27) and the transformation relations (19), we obtain the velocities of the internal motion:

$$\begin{aligned} u &= \frac{1}{2}v\eta^2 r e^{-\eta z} \\ w &= -v\eta(1 - e^{-\eta z}) \end{aligned} \quad (28)$$

where $\eta = 1.503(\kappa/\nu)^{1/2}$ has a unit of inverse length. Note that $1/\eta$ is the characteristic length in the present problem and represents the ‘boundary layer thickness’ of the droplet internal motion from the impacting interface, beyond which viscous loss can be neglected.

5. Intervening Gas Flow

For the intervening gas flow between two impacting interfaces, the characteristic length is the gap distance, which can reach a value of the order of 10^{-8} m or less before merging. Since the mean free path in one atmosphere is about 10^{-7} m, the Knudsen number, which is defined as the ratio of the mean free path to the characteristic length, can be as large as $O(10)$. It is therefore clear that, during the entire process of droplet collision, the intervening gas flow experiences a wide range of flow regimes, from continuum ($Kn < 10^{-3}$), to slip flow ($10^{-3} < Kn < 10^{-1}$), to transition ($10^{-1} < Kn < 10$), and finally to free molecular flow ($Kn > 10$). Accordingly, the effect of rarefied gas must be considered in our formulation in order to correctly estimate the gap pressure distribution, which is crucial for calculating the resistance force on the droplet by the gap flow.

5.1 Continuum Flow Solution based on Lubrication Theory

In most situations, the droplets do not suffer significant deformation until the separation distance between the droplets is much smaller than the droplet radius. If the separation distance is also much larger than the mean free path, lubrication theory for continuum flows is applicable to

describe the intervening gas flow [18] during the early stage of droplet collision. The solution provides useful scaling results on the flow variables as well as the initial condition for the present problem; the latter will be shown in Section 5.

For the lubrication flow between two flattened disc-shaped interfaces, the radial dimension a is much larger than the axial dimension h , and the radial velocity gradient is negligibly small compared to the axial velocity gradient. The pressure across the gap is approximately constant so that it is only a function of the radial position. Thus the momentum equation of the lubrication flow is given by

$$\mu_g \frac{\partial^2 u}{\partial z^2} = \frac{dp}{dr} \quad (29)$$

and the incompressible continuity equation is given by

$$\frac{1}{r} \frac{\partial}{\partial r}(ru) + \frac{\partial w}{\partial z} = 0 \quad (30)$$

The boundary conditions are

$$\left. \frac{\partial u}{\partial z} \right|_{z=0} = 0, \quad u|_{z=\pm h/2} = \kappa r \quad (31)$$

$$w|_{z=0} = 0, \quad w|_{z=\pm h/2} = \frac{d(\pm h/2)}{dt} \quad (32)$$

$$\left. \frac{dp}{dr} \right|_{r=0} = 0, \quad p|_{r=a} = p_0 \quad (33)$$

where κr represents the tangential velocity of the interfaces because of the no-slip boundary condition, and p_0 is the ambient pressure that can be absorbed in p since only the pressure difference is of interest.

The solution of equations (29)~(33) yields the lubrication pressure

$$p = \frac{3\mu_g}{h^3} (r^2 - a^2) \left(\frac{dh}{dt} + 2\kappa h \right) \quad (34)$$

and the resistance force calculated from (5) is

$$F = -\frac{3\pi\mu_g a^4}{2h^3} \left(\frac{dh}{dt} + 2\kappa h \right) \quad (35)$$

For the undeformed spherical droplet, the governing equations are still given by (29) and (30). However, the impacting interfaces are not flat, but are approximately described by $H(r, t) = h(t) + r^2/R_0$ [18, 19], where h is the distance between the two interfaces along the symmetric axis, and R_0 is the radius of the spherical droplets. The lubrication pressure is given by

$$p = -\frac{3\mu_g R_0}{2(h + r^2/R_0)^2} \frac{dh}{dt} \quad (36)$$

and the resistance force by

$$F = -\frac{3\pi\mu_g R_0}{2h} \frac{dh}{dt} \quad (37)$$

From (35) and (37), we can see that the resistance force for a flattened droplet is inversely proportional to h^3 , while it is inversely proportional to h for a rigid spherical droplet. This difference can be used to explain the coalescence of droplets for very small Weber numbers ($We \ll 1$), where the droplet deviates only weakly from its original spherical shapes. The slowly increasing ($\propto 1/h$) resistance force allows the droplets to be sufficiently close so that coalescence always happens. When the droplet deformation is large, the flattened droplets experience a more rapid increase in the resistance force ($\propto 1/h^3$) and are quickly decelerated so that coalescence is less favored. Consequently, since for collision at large Weber numbers the droplets gradually deform from their initially spherical shape, it is reasonable to expect that the droplets will experience a relatively fast approaching stage characterized with a slowly increasing resistance force ($\propto 1/h$), and then a relatively slow approaching stage characterized by a rapidly increasing resistance force ($\propto 1/h^3$). If coalescence is favored, the droplets will then experience another fast approaching stage due to the rapidly increasing molecular attractive force that is $\propto 1/h^3$, to be shown in Section 5.3.

It is noted that the effect of the inertia of the intervening gas is neglected and the flow is considered to be quasi-steady in lubrication theory. As a result, the dynamics of the droplet is decoupled from the intervening gas flow if we also neglect the pressure balance between the liquid and gas. This pressure difference can actually be used to calculate the shape of the interface phases by using the normal stress balance. The boundary integral theory is a widely used method to study the evolution of interfaces [20, 21, 22]. In the present study, we neglect the effect of the very small interfacial curvature by assuming the interfaces to be flat.

5.2 Rarefied Flow Solution based on Boltzmann Equation

Sundararajakumar & Koch [23] studied the rarefied gas flow between two spheres under conditions of small Mach number. They showed that the gap flow between two spherical impacting interfaces can be approximated locally as a Poiseuille flow between two flat plates, and the effect of the rarefied gas can be considered by replacing the continuum radial flux by a solution of the linearized Boltzmann equation. Then the pressure drop required to achieve the radial flux is obtained by mass conservation. In the present situation, the droplet interface has been sufficiently flattened when the gap distance reaches the range where the effect of rarefied gas cannot be neglected. The radius of the flattened surface is much larger (about 10^2 times or more) than the gap thickness. Consequently, the planar Poiseuille flow adequately approximates the gap flow between two flat interfaces instead of just being locally approximate. However, different from the pure Poiseuille rarefied flows [24, 25], the flattened interfaces expand on their own planes so that the effect of tangential velocity must be considered. It is noted that although the planar Poiseuille flow in rarefied gas dynamics is not a very difficult problem in the near

continuum and the free-molecular regimes, the present problem requires a general solution for the entire range of the Knudsen number, from the continuum to the free-molecular flows.

In this section, the rarefied gas flow between two flattened interfaces will be analyzed, with particular interests in studying the effects of the tangential velocity of the interfaces and in deriving an expression for the pressure distribution over the entire Knudsen number range.

The Boltzmann equation in cylindrical coordinates (r, ϕ, z) is given by [26]

$$\frac{\partial f}{\partial t} + \xi_r \frac{\partial f}{\partial r} + \frac{\xi_\phi}{r} \frac{\partial f}{\partial \phi} + \xi_z \frac{\partial f}{\partial z} + \frac{\xi_\phi^2}{r} \frac{\partial f}{\partial \xi_r} - \frac{\xi_r \xi_\phi}{r} \frac{\partial f}{\partial \xi_\phi} = J(f, f) \quad (38)$$

in the absence of external forces, where $f = f(t, \mathbf{x}, \boldsymbol{\xi})$ is the distribution function, $\boldsymbol{\xi}$ the velocity of the molecules, and $J(f, f)$ the nonlinear collision integral.

Because the radius of the disk is much larger than the gas film thickness, that is $R \gg h$, we neglect all the terms containing $1/r$. Consequently, the Boltzmann equation for the quasi-steady, axisymmetric flow in the thin gas gap can be approximated as

$$\xi_r \frac{\partial f}{\partial r} + \xi_z \frac{\partial f}{\partial z} = J(f, f) \quad (39)$$

To describe the collision integral, we use the BGK approximation [27], which is essentially a nonlinear relaxation formulation:

$$J(f, f) = (f_0 - f)/\tau_c \quad (40)$$

In (40) f_0 is the local Maxwellian distribution defined as

$$f_0 = n \left(\frac{m}{2\pi kT} \right)^{3/2} \exp \left[-\frac{m}{2kT} (\boldsymbol{\xi} - \mathbf{u})^2 \right] \quad (41)$$

where the local number density n , the local temperature T and the local flow velocity \mathbf{u} are integrals of the undetermined distribution function f , and τ_c represents a characteristic relaxation time that is equal to the time between the molecular collisions.

For the boundary conditions, we assume that the molecules reflected from the wall have a local Maxwellian distribution such that the accommodation coefficient is unity:

$$f(r, z = \pm h/2) = n_w(r) \left(\frac{m}{2\pi kT_w} \right)^{3/2} \exp \left[-\frac{m}{2kT_w} (\boldsymbol{\xi} - \mathbf{u}_w)^2 \right] \quad (42)$$

where the subscript ‘w’ indicates properties evaluated at the wall. In the present problem, the wall velocity is given by

$$\mathbf{u}_w = u_w \mathbf{e}_r = \kappa r \mathbf{e}_r \quad (43)$$

where \mathbf{e}_r is the unit vector in the radial direction.

Given that the mean flow velocity is much smaller than the speed of sound, the nonlinear Boltzmann equation can be linearized [26, 23]. Thus we first linearize the distribution function by

$$f = f_{00}(1 + \varphi) \quad (44)$$

where

$$f_{00} = n_0 \left(\frac{m}{2\pi k T_0} \right)^{3/2} \exp \left(-\frac{m}{2k T_0} \xi^2 \right), \quad \varphi = \varphi(t, \mathbf{x}, \xi) \ll 1 \quad (45)$$

where n_0 and T_0 are the number density and temperature, respectively, at the symmetric center (see Figure 5.1). The number density and the temperature can also be linearized as

$$n(z) = n_0[1 + \nu(z)], \quad T(z) = T_0[1 + \tau(z)] \quad (46)$$

By using (44) and (46), the linearized Boltzmann equation with the linearized BGK formulation is given by

$$\frac{v_r}{\alpha} \frac{\partial \varphi}{\partial r} + \frac{v_z}{\alpha} \frac{\partial \varphi}{\partial z} = -\varphi + \nu + 2u_1 v_r + (v^2 - 3/2)\tau \quad (47)$$

where $\mathbf{v} = \xi(m/2kT_0)^{1/2}$ is the dimensionless molecule velocity; z has been scaled by h , the gas film thickness; $\alpha = 1/Kn$ is the inverse Knudsen number; and $u_1 = u_r(m/2kT_0)^{1/2}$ is the dimensionless radial flow velocity.

The boundary conditions are given by

$$\varphi(r, z = \pm h/2) = \nu + 2u_{1w} v_r \quad (48)$$

where $u_{1w} = u_w(m/2kT_0)^{1/2}$ is the dimensionless wall velocity.

Assuming that the flow is isothermal ($\tau \equiv 0$), and introducing a separation of variable transformation (u_{1w} is a slow variable along the radial direction),

$$\varphi = -Kr + 2u_{1w} v_z \psi(z, \xi) \quad (49)$$

where $K(r) = -(dp/dr)/p_0$ is the relative local pressure gradient, we obtain

$$\frac{v_z}{\alpha} \frac{\partial \psi}{\partial z} = -\psi + \frac{hK}{\alpha u_{1w}} + \frac{2u_1}{u_{1w}} \quad (50)$$

with the boundary conditions

$$\psi(z = \pm \frac{1}{2}) = 1 \quad (51)$$

Equation (50) has a solution in an integral form:

$$\psi^\pm(z) = \exp\left(-\alpha \frac{z \pm \frac{1}{2}}{v_z}\right) + \alpha \int_{\mp \frac{1}{2}}^z \left(\frac{hK}{\alpha u_{1w}} + \frac{2u_1}{u_{1w}}\right) \frac{1}{v_z} \exp\left(-\alpha \frac{z-s}{v_z}\right) ds \quad (52)$$

where ψ^+ denotes the distribution function corresponding to $v_z > 0$, ψ^- denotes the distribution function corresponding to $v_z < 0$, and use has been made of the boundary conditions (51).

Multiply both sides of (52) by $\pi^{-3/2} v_r^2 \exp(-v^2)$, and integrate the resulting expression with respect to v from zero to infinity, we obtain

$$u_1(z) = \frac{u_{1w}}{2\sqrt{\pi}} \left[J_0\left(\alpha\left(\frac{1}{2}+z\right)\right) + J_0\left(\alpha\left(\frac{1}{2}-z\right)\right) \right] + \frac{\alpha}{\sqrt{\pi}} \int_{-1/2}^{1/2} \left(\frac{hK}{2\alpha} + u_1\right) J_{-1}(\alpha|z-s|) ds \quad (53)$$

where J_0 and J_{-1} is a special function defined by the integral

$$J_m(x) = \int_0^\infty \xi^m e^{-\xi^2 - \frac{x}{\xi}} d\xi \quad (54)$$

which has been studied by Abramowitz [28] and Laporte [29].

Introducing the transformation

$$u(z) = \frac{u_{1w}}{2} + \frac{hK}{2\alpha} [\Psi(z) - 1] \quad (55)$$

(53) becomes

$$\Psi(z) = 1 + \frac{\alpha}{\sqrt{\pi}} \int_{-1/2}^{1/2} \Psi(s) J_{-1}(\alpha|z-s|) ds \quad (56)$$

which is exactly the same equation derived by Cercignani & Daneri [24] for a pure Poiesulle flow.

The special function $J_{-1}(x)$ has a logarithmic singularity at $x = 0$. It is therefore expected that, based on the concept of saddle point approximation, the major contribution to the value of the integral (56) comes from the neighborhood of $s = z$. We can therefore write (56) as

$$\Psi(z) = 1 + \frac{\alpha}{\sqrt{\pi}} \Psi(z) \int_{-1/2}^{1/2} J_{-1}(\alpha|z-s|) ds \quad (57)$$

Solving $\Psi(z)$ from (57) and substituting it into (55), we obtain

$$u(z) = \frac{u_{1w}}{2} + \frac{hK}{2\alpha} \left[\frac{\sqrt{\pi}}{J_0\left[\alpha\left(\frac{1}{2}+z\right)\right] + J_0\left[\alpha\left(\frac{1}{2}-z\right)\right]} \right] \quad (58)$$

Cercignani & Daneri [24] solved (56) numerically and tabulated the results for $0.01 < \alpha < 10$. For the cases $\alpha < 0.01$ and $\alpha > 10$, two asymptotic solutions were derived. The approximate solution (58) derived herein shows very good agreement with Cercignani's numerical solution [24] for $\alpha \leq 1$. For large α , the saddle point method used to derive (57) is not uniformly valid for all z .

Actually, there exist two very thin Knudsen layers next to the walls ($z = \pm 1/2$). Outside these Knudsen layers, the solution asymptotically converges to the continuum solution

$$\Psi(z) = 1 - \alpha^2 z^2 + c_2 z + c_3 \quad (59)$$

where the constants c_2 and c_3 can be determined by the slip boundary conditions at $z = \pm 1/2$, which are given by solving (56) in the Knudsen layers.

The solution of (56) in the Knudsen layers and the derivation of the slip boundary conditions have been studied by Welander [30], Willis [31], and Cercignani [32]. If we introduce a coordinate transformation

$$\alpha(1/2 - z) = \eta; \quad \alpha(1/2 + z) = \alpha - \eta \quad (60)$$

and realize that the first approximation solution in the Knudsen layers should be like

$$G(\eta) = \frac{1}{\alpha} [\psi(z) - (1 - \alpha^2 z^2 + c_2 z + c_3)] \quad (61)$$

we obtain

$$G(\eta) = \frac{1}{\sqrt{\pi}} \int_0^\infty G(\eta') J_{-1}(|\eta - \eta'|) d\eta' \quad (62)$$

This is the Wiener-Hopf integral equation whose solution can be obtained through standard, albeit complicated process [30, 31]. Since we are not interested in the detailed structure of the Knudsen layer, and recognizing that there is no analytical solution for that, we shall obtain a modification of the outer solution, i.e., the slip velocity that is given by [24, 33]

$$G(\eta = \infty) = 1.012 \quad (63)$$

Consequently, the final solution for (59) is

$$\psi(z) = 1 - \alpha^2 (z^2 - 1/4) + 1.012\alpha \quad (64)$$

and the radial velocity is given by substituting (64) into (55):

$$u_1(z) = \frac{u_w}{2} + \frac{hK}{2\alpha} [-\alpha^2 (z^2 - 1/4) + 1.012\alpha] \quad (65)$$

The mass conservation equation can be derived by averaging the Boltzmann equation over the velocity space

$$\frac{1}{r} \frac{\partial}{\partial r} (r \rho u) + \frac{\partial}{\partial z} (\rho w) = 0 \quad (66)$$

Integrating (66) across the gap from $-h/2$ to $h/2$ yields

$$\rho \frac{dh}{dt} + \frac{1}{r} \frac{\partial}{\partial r} (r \rho j) = 0, \quad j = \int_{-h/2}^{h/2} u dz \quad (67)$$

where j represents the pressure-driven radial volumetric flux of the gas in the gap.

By applying the velocity solution (58) and (65) to (67), we obtain the pressure within the gap,

$$p = \frac{3\mu_g}{h^3} (r^2 - a^2) \left(\frac{dh}{dt} + 2\kappa h \right) \frac{1}{f(Kn)} \quad (68)$$

where

$$f(Kn) = 6Kn^2 \left[\int_{-1/2}^{+1/2} \frac{\sqrt{\pi}}{J_0\left(\frac{1/2-x}{Kn}\right) + J_0\left(\frac{1/2+x}{Kn}\right)} dx - 1 \right] \quad Kn \geq 1 \quad (69)$$

$$f(Kn) = 1 + 6\sigma Kn \quad (\sigma = 1.012) \quad Kn \ll 1 \quad (70)$$

Considering that (69) is very accurate for $Kn \geq 1$, we shall use

$$f(Kn) = 1 + 6\sigma Kn + c_1 Kn^2 + c_2 Kn^3 \quad (71)$$

instead of (70) to match (69) by making the values and the first order derivatives of (69) and (71) continuous at the point $Kn = 1.0$. The resulting matching coefficients are

$$c_1 = 0.9650, \quad c_2 = 0.6967 \quad (72)$$

It is noted that (71) can be regarded as a higher order approximation than (70).

By numerically integrating (69), we find that the results can be correlated quite well by a linear function in a log-log scale:

$$\log_{10}[f(Kn)] = 1.1551(\log_{10} Kn) + \log_{10} 8.7583 \quad (73)$$

Both (69) and (73) are compared in Figure 5.1.

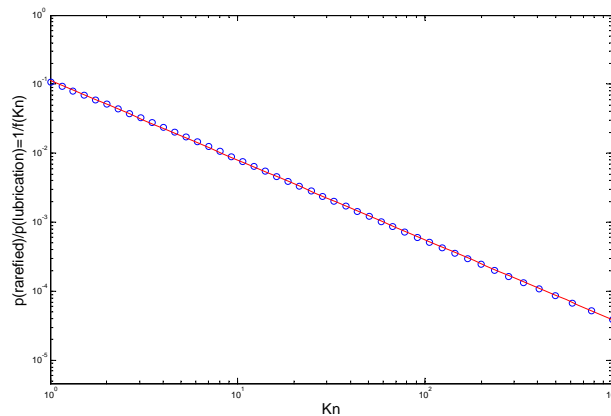


Figure 5.1 The variation of the pressure correction due to the rarefied gas effect with the Knudsen number ($Kn \geq 1$). Comparison of the numerical integration of (69) (blue circle) with the linear correlation function (73) (red line) in the log-log scale.

Combining (71) and (73), we obtain the following expression,

$$f(Kn) = \begin{cases} 1 + 6.0966Kn + 0.9650Kn^2 + 0.6967Kn^3 & Kn \leq 1 \\ 8.7583Kn^{1.1551} & Kn > 1 \end{cases} \quad (74)$$

The numerical results of (74) are shown in Figure 5.2, together with (69) and (70) for comparison.

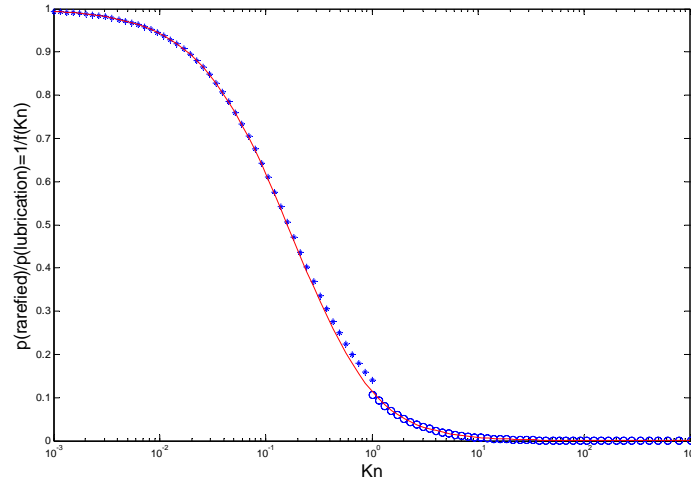


Figure 5.2 The variation of the pressure correction due to the rarefied gas effect with the Knudsen number. Comparison between the numerical integration of (69) for $Kn \geq 1$ (blue circle), the first approximation (70) for $Kn \ll 1$, which is extended to $Kn = 1$ (blue asterisk) and the composite expression (74) by matching (69) and (70) (red line).

5.3 Molecular Attraction Force

The influence of the van der Waals force can be incorporated in the formulation by adding a ‘negative’ pressure at the droplet surface [10]

$$P_{vdW} = \frac{A}{6\pi h^3} \quad (75)$$

where A is the Hamaker constant [34]. The magnitude of A is generally between $10^{-21} \sim 10^{-18}$ J, which implies that the van der Waals force is negligible unless the gap distance is small enough. Once the van der Waals force starts to play an important role, it increases with h very rapidly as $1/h^3$ and hence dominates over other forces.

Consequently, the pressure appearing in the droplet dynamics is given by

$$p = p_{gas} + P_{vdW} \quad (76)$$

where p_{gas} is the gas pressure we derived in Section 5.2.

6. The Initial Value Problem of Droplet Dynamics

By using the results from Sections 4 and 5, the viscous dissipation term given by (10) and the resistance force by (5) can be determined. We thus obtain the following nondimensional ODE system, characterized by four unknowns a , b , R and h that are normalized by R_0 , and the independent variable time, t , normalized by R_0/V_0 .

The geometric relation (1) leads to a differential relation between a , b and R :

$$\hat{a}\hat{a}' + \hat{b}\hat{b}' = \hat{R}\hat{R}' \quad (77)$$

where the superscript “ $\hat{\cdot}$ ” represents the corresponding nondimensional variable and the superscript “ $'$ ” represents the derivative with respect to the nondimensional time.

The overall mass conservation (2) leads to an additional relation between b and R :

$$\hat{R}' = -\frac{\hat{R}-\hat{b}}{2\hat{R}}\hat{b}' \quad (78)$$

The energy balance (6) leads to a second order ODE for G :

$$\hat{G}'' = -\frac{15}{\text{Re}_l^3} \frac{1}{\hat{G}'} \left[\frac{\hat{R}^2 - \hat{b}^2}{2} \hat{\eta}^3 + \frac{\hat{b}}{2} \hat{\eta}^2 - \frac{1}{4} \hat{\eta} + \left(\frac{\hat{R}}{2} \hat{\eta}^2 + \frac{1}{4} \hat{\eta} \right) e^{-2\hat{\eta}(\hat{R}+\hat{b})} \right] - \frac{3}{\text{We}} \frac{1}{\hat{G}'} (\hat{R} + \hat{b}) \hat{R}' \quad (79)$$

where G is related to b and R through

$$\hat{G}' = \left[1 - \frac{3(\hat{R}-\hat{b})}{2(2\hat{R}-\hat{b})} \right] \hat{b}' \quad (80)$$

and

$$\hat{G}'' = \left[1 - \frac{3(\hat{R}-\hat{b})}{2(2\hat{R}-\hat{b})} \right] \hat{b}'' + \frac{3(\hat{R}+\hat{b})}{2\hat{R}(2\hat{R}-\hat{b})} (\hat{b}')^2 \quad (81)$$

The first term on the RHS of (79) represents the viscous dissipation where $\text{Re}_l = 2\rho_l R_0 V_0 / \mu_l$ is the Reynolds number of the droplet, and

$$\hat{\eta} = 1.503(\text{Re}_l/2)^{1/2} \sqrt{\hat{\kappa}} = 1.503(\text{Re}_l/2)^{1/2} \sqrt{\frac{1}{\hat{a}} \frac{d\hat{a}}{d\hat{t}}} \quad (82)$$

The second term represents the surface energy where $\text{We} = 8\rho_l R_0 (V_0)^2 / \sigma$ is the Weber number of the droplet,

The Newton's equation of motion (3) leads to

$$\hat{h}' = -\frac{4}{9} \frac{\hat{h}^3}{\hat{a}^4} \frac{\text{Re}_g}{\varepsilon} \frac{1}{f(Kn)} \left(\hat{G}'' + \hat{A} \frac{\hat{a}^2}{\hat{h}^3} \right) - 2\hat{\kappa}\hat{h} \quad (83)$$

where $Re_g = 2\rho_g R_0 V_0 / \mu_g$ is the Reynolds number of the gas, $\varepsilon = \rho_g / \rho_l$ is the gas-to-liquid density ratio, and $\hat{A} = A / [8\pi\rho_l (V_0)^2 (R_0)^3]$ is the nondimensional Hamaker constant. The fact that $|G''| \gg |h''|$ has been used to obtain (83).

To specify the initial conditions for the system of ODEs, we first recognize that the droplets in the present formulation are assumed to be deformed liquid spheres with flattened disc-shaped interfaces whose radius is much larger than the gap distance between the two interfaces. Obviously, this assumption is not configurationally correct in the very beginning stage of droplet collision, at which the flattened interface has not been formed. Thus an independent specification is needed for the initial configuration. This specification can be acquired through either numerical simulation of the collision dynamics to a state at which the flattened disk is formed and the continuum formulation is still valid, or an asymptotic analysis based on weakly deformed droplets. We shall however identify an appropriate initial configuration through a phenomenological consideration, as follows.

If the gap distance between the two undeformed droplets is small enough so that the lubrication theory can be applied, each spherical droplet experiences the repulsive force given by (37). Thus, by solving the equation of droplet motion

$$M \frac{d^2 h}{dt^2} = -\frac{3\pi\mu_g R_0}{2h} \frac{dh}{dt} \quad (84)$$

subject to the initial conditions

$$h|_{t=0} = h_0, \quad \left. \frac{dh}{dt} \right|_{t=0} = -V_0 \quad (85)$$

where h_0 is sufficiently small to make the lubrication theory applicable, and V_0 is the initial impact velocity, we obtain

$$\frac{dh}{dt} = -\frac{3\pi\mu_g R_0}{2M} \ln \frac{h}{h_0} - V_0 \quad (86)$$

Then, we obtain the characteristic pressure at $r = 0$ by substituting (86) into (36) and letting $r = 0$

$$p = \frac{3\mu_g R_0}{2h^2} \left(\frac{3\pi\mu_g R_0}{2M} \ln \frac{h}{h_0} + V_0 \right) \quad (87)$$

We next recognize that the droplet begins to deform significantly when the intervening gas pressure (87) exceeds the surface tension.

$$p = \frac{2\sigma}{R_0} \quad (88)$$

Thus, we may consider that the interfaces of the two droplets are flattened when the following condition is satisfied

$$\frac{3\mu_g R_0}{2h_c^2} \left(\frac{3\pi\mu_g R_0}{2M} \ln \frac{h_c}{h_0} + V_0 \right) = \frac{2\sigma}{R_0} \quad (89)$$

from which, we obtain

$$\frac{h_c}{h_0} = \frac{2M}{3\pi\mu_g R_0} \left(\frac{2\sigma}{R_0} - \frac{2h_c^2}{3\mu_g R_0} - V_0 \right) \quad (90)$$

Since $h_c \ll h_0$, the critical gap distance h_c satisfying (90) can be approximated by

$$h_c = R_0 \sqrt{\frac{3\mu_g V_0}{2\sigma}} \quad (91)$$

or its nondimensional form

$$\hat{h}_c = \sqrt{\frac{3\mu_g V_0}{2\sigma}} = \sqrt{3Ca/2} \quad (92)$$

where Ca is the capillary number, which is typically about $O(10^{-3})$ in the present problem. Equation (92) implies that significant deformation of the droplet is prevented until the minimum separation between two droplets is much smaller than their radius.

The characteristic pressure for a flattened droplet is given by setting $h = h_c$, $r=0$, $dh/dt = -V_0$ and $\kappa=0$ in (34):

$$p = \frac{3\mu_g}{h_c^3} a^2 V_0 \quad (93)$$

We assume that the pressure is approximately constant during the initial deformation process, and use (93) and (88) to determine the radius of the flattened disk. Thus, we have

$$\frac{3\mu_g}{h_c^3} a^2 V_0 = \frac{2\sigma}{R_0} \quad (94)$$

which gives

$$\hat{a}_c = \sqrt{\hat{h}_c} \quad (95)$$

Droplet deformation has been investigated previously in two situations, namely, constant approach force [20, 21] and constant approach velocity [35], which is appropriate for the present problem. Klaseboer et. al. [36] found the radius of the flattened interfaces as a function of time:

$$\hat{a} = \sqrt{\hat{t}}/2 \quad (96)$$

By considering simultaneously (95) and (96), we obtain the typical deformation time as

$$\hat{t}_c \propto \hat{h}_c \quad (97)$$

In fact, during this period the two droplets still approach each other according to [17, 19]

$$\hat{h} \propto \exp(-\hat{t}) \quad (98)$$

By using (92), (95), (97) and (98), we obtain the initial conditions for the above ODE system,

$$\hat{h}_0 = \sqrt{3Ca/2} \exp(-\alpha\sqrt{3Ca/2}) \quad (99)$$

$$\hat{a}_0 = \sqrt{\hat{h}_0} \quad (100)$$

$$\hat{b}_0 = \sqrt{1 - \hat{a}_0^2} \quad (101)$$

$$\hat{R}_0 \approx 1 \quad (102)$$

where the empirical coefficient α can be given by numerical simulation or asymptotic analysis. Klaseboer et. al. [36] experimentally found α to be about 40. In the present study, we have used $\alpha = 47.5$ for tetradecane and $\alpha = 105.0$ for water, obtained by trial and error so that the present theory can predict all of the experimental observation in different ambient pressures. Compared with tetradecane, water has larger surface tension and is harder to deform, it is therefore expected that water droplets need more time to be flattened. The ratio of the α for water to that for tetradecane is close to the ratio of their surface tension. Further study on eliminating the empirical nature of α is under consideration.

7. Results and Discussion

The Livermore ODE solver LSODE is used to solve the system (77)~(83), which is found to be stiff. Collisions of water and tetradecane droplets were studied. The physical properties of ambient air, water and tetradecane are listed in Table 7.1.

Table 7.1 Physical properties of ambient air, water and tetradecane

	Density (kg/m ³)	Viscosity (N·s/m ²)	Surface tension (N/m)	Hamaker constant (10 ⁻²⁰ J)
Air (1.0 atm)	1.00	1.98×10 ⁻⁵	\	\
Water	1.00×10 ³	1.00×10 ⁻³	7.28×10 ⁻²	5.1
Tetradecane	0.73×10 ³	2.18×10 ⁻³	2.70×10 ⁻²	3.7

Figure 7.1 shows the evolution of the gap thickness with time for the collision of tetradecane droplets in one atmosphere air. It is seen that for small values of the collision Weber number, say $We = 1.5$, the approaching interface leads to a steady and then an accelerative decrease in h , hence signifying the occurrence of coalescence. However, as We is increased to 1.8, the approaching interface eventually retracts, thereby signifying bouncing. Subsequently, coalescence occurs again as We is further increased to 23.0. Experimental values for the

transition We are 2.3 and 12.3, respectively. Recognizing the complexity of the present theory, the theoretical transition We determined herein can be considered to be acceptable.

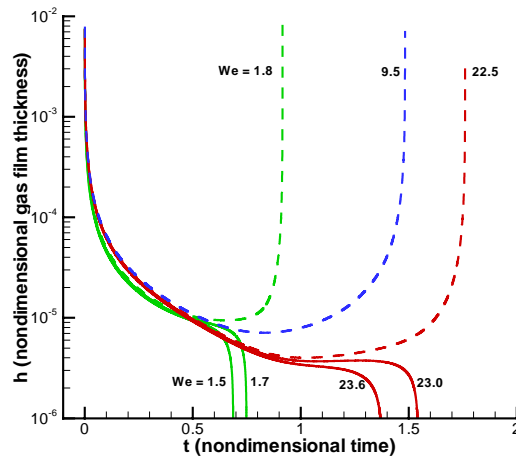


Figure 7.1 The evolution of the gap width with time for the collision of tetradecane droplets in one atmosphere air

Figures 7.2 and 7.3 show the evolution of the gap thickness with time for tetradecane droplets in reduced (0.6atm) and elevated (2.4atm) pressures, respectively. In the reduced pressure environment, the gas between two droplets has a lower density and is readily squeezed out so that coalescence is apt to happen, as shown in Figure 7.2. On the contrary, in an elevated pressure environment, the denser gas between the two droplets is harder to be squeezed out. It will be trapped in the gap, leading to substantial pressure buildup and hence droplet deformation. As a result, the soft coalescence characterized by small deformation is absent in elevated pressure environment, as shown in Figure 7.3. These theoretical results therefore substantiate the previous experimental observations [5].

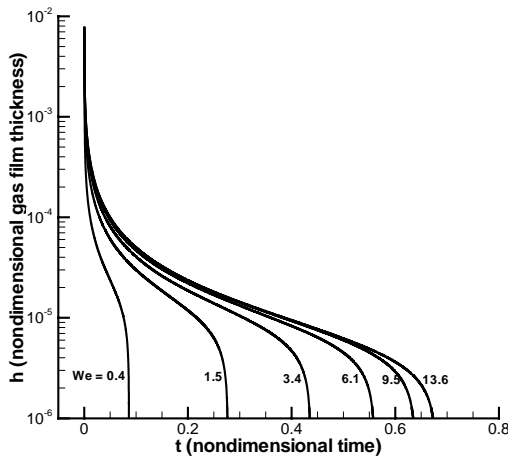


Figure 7.2 The evolution of the gap width with time for the collision of tetradecane droplets in 0.6 atmosphere air.

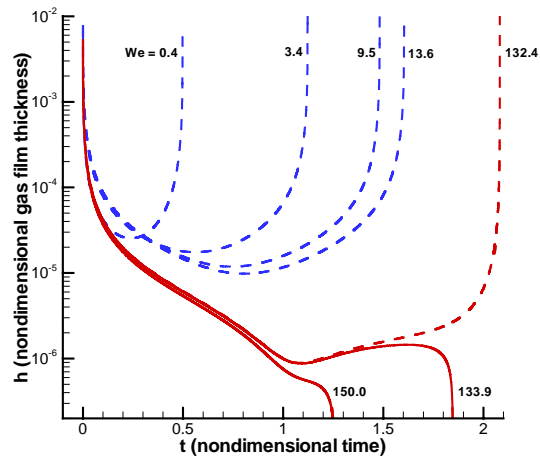


Figure 7.3 The evolution of the gap width with time for the collision of tetradecane droplets in 2.4 atmosphere air.

Figures 7.4~7.6 show the evolution of the gap width with time for water droplets in 1.0, 2.7 and 8.0atm, respectively. It is seen that while bouncing is absent for water droplets at one atmosphere (Figure 7.4), it occurs at higher pressures as shown in Figs. 7.5 and 7.6. The non-monotonic transition from coalescence to bouncing to coalescence again occurs for water droplets in 2.7atm, while the soft coalescence is absent in 8.0atm. These theoretical results are again in agreement with the experimental observations of Qian & Law [5].

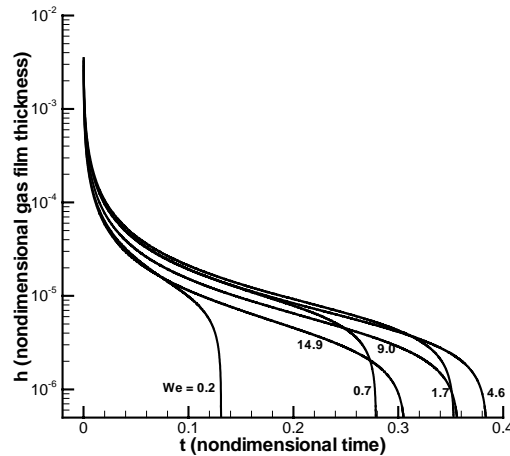


Figure 7.4 The evolution of the gap width with time for the collision of water droplets in one atmosphere air.

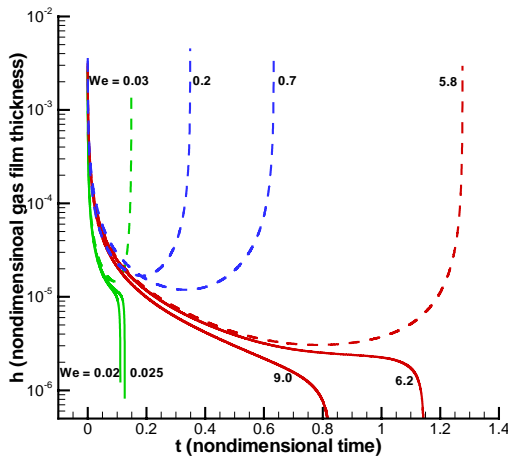


Figure 7.5 The evolution of the gap width with time for the collision of water droplets in 2.7 atmosphere air.

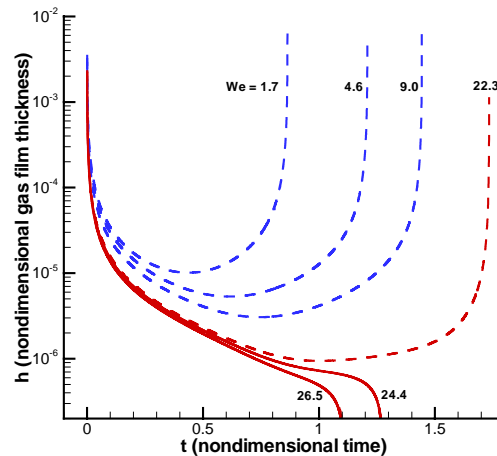


Figure 7.6 The evolution of the gap width with time for the collision of water droplets in 8.0 atmosphere air.

8. Concluding Remarks

In the present investigation we have formulated a comprehensive theory of head-on droplet collision that can successfully describe coalescence and bouncing outcomes, allowing for the large-scale droplet deformation, viscous loss through internal motion, rarefied flow effects of the intervening gas between the colliding interfaces, and van der Waals force that destroys and hence

causes merging of the interfaces. Of particular merit is the verification of the experimental observation that, with increasing impact inertia, droplet collision could result in the nonmonotonic response of coalescence, bouncing, and coalescence again. The distinctively different outcome of water versus hydrocarbon droplets at different environment pressures is also theoretically confirmed. Furthermore, as a consequence of the present investigation, individual theories have been developed for the component processes of the stagnation boundary layer flow with an expanding stagnation surface, and rarefied Poiseuille flow with a tangentially stretched surface.

The present study can also be extended to phenomena of this nature, such as off-centered collisions, collisions involving droplets of unequal sizes or different materials, droplet impacting a rigid surface which is either dry or has been wetted by the arrival of previous droplets, collision of micron- or nano-sized droplets, and bubble dynamics. The usefulness of the present theory to diverse applications involving multi-phase flows is also evident.

Acknowledgement

This work was supported by the Air Force Office of Scientific Research under the technical monitoring of Dr. Mitat Birkan.

References

- [1] Adam, J. R. and Lindblad, N. R. 1968 The collision, coalescence, and disruption of water droplets. *Appl. Phys.* **39**, 173.
- [2] Brazier-Smith, P. R., Jennings, S.G. & Latham, J. 1972 The interaction of falling water drops: coalescence. *Proc. R. Soc. Lond. A* **326**, 393.
- [3] Ashgriz, N. and Poo, J. Y. 1990 Coalescence and separation in binary collision of liquid drops. *J. Fluid Mech.* **221**, 183.
- [4] Jiang, Y. J., Umemura, A. & Law, C. K. 1992 An experimental investigation on the collision behaviour of hydrocarbon droplets. *J. Fluid Mech.* **234**, 171.
- [5] Qian, J. and Law, C. K. 1997 Regimes of coalescence and separation in droplet collision. *J. Fluid Mech.* **331**, 59.
- [6] Roisman, I. V. 2004 Dynamics of inertia dominated binary drop collision. *Phys. Fluids*. **16**, 3438.
- [7] Gopinath, A. and Koch, D. L. 2002 Collision and rebound of small droplets in an incompressible continuum gas. *J. Fluid Mech.* **454**, 145.
- [8] Bach, G. A., Koch, D. L. and Gopinath, A. 2004 Coalescence and bouncing of small aerosol droplets. *J. Fluid Mech.* **518**, 157.
- [9] Mackay, G.D. & Mason, S. G. 1963 The gravity approach and coalescence of fluid drops at liquid interfaces. *Can. J. Chem. Engng* **41**, 203.
- [10] Pan, K. L. 2004 Dynamics of droplet collision and flame-front motion, Ph.D thesis, Princeton University.
- [11] Dai, M. and Schmidt, D. P. 2005 Numerical simulation of head-on droplet collision: effect of viscosity on maximum deformation. *Phys. Fluids*. **17**, 041701.
- [12] White, F. M. 1991 *Viscous Fluid Flow* (2nd ed.), McGraw-Hill Inc.
- [13] Bradley, S. G. and Stow, C. D. 1978 Collisions between liquid drops. *Phil. Trans. R. Soc. Lond. A* **287**, 635.
- [14] Th. von Kármán, 1921 On laminar and turbulent friction. NACA-TM-1092.
- [15] Coltrin, M. E., Kee, R. J. and Evans, G. H. 1989 A mathematical model of the fluid mechanics and gas-phase chemistry in a rotating disk chemical vapor deposition. *J. Electrochem. Soc.* **136**, 819.
- [16] Meksyn, D. 1961 *New Methods in Laminar Boundary-Layer Theory*. New York, Pergamon Press.
- [17] Schlichting, H. 1968 *Boundary Layer Theory*. McGraw-Hill Inc.
- [18] Davis, R. H., Schonberg, J. A. and Rallison, J. M. 1989 The lubrication force between two viscous drops. *Phys. Fluids A*. **1**, 77.

- [19] Kytömaa, H. K. and Schmid, P. J. 1992 On the collision of rigid spheres in a weakly compressible fluid. *Phys. Fluids A*, **4**, 2683.
- [20] Yiantsios, S. G. and Davis, R. H. 1990 On the buoyancy-driven motion of a drop towards a rigid surface or a deformable interface. *J. Fluid Mech.* **217**, 547.
- [21] Yiantsios, S. G. and Davis, R. H. 1991 Close approach and deformation of two viscous drops due to gravity and van der Waals forces. *J. Coll. Interface Sci.* **144**, 412.
- [22] Janssen, P. J. A., Anderson, P. D., Peters, G. W. M. and Meijer, H. E. H. 2006 Axisymmetric boundary integral simulations of film drainage between two viscous drops. *J. Fluid Mech.* **567**, 65.
- [23] Sundararajakumar, R. R. and Koch, D. L. 1996 Non-continuum lubrication flows between particles colliding in a gas. *J. Fluid Mech.* **313**, 283.
- [24] Cercignani, C. and Daneri, A. 1963 Flow of a rarefied gas between two parallel plates. *J. App. Phys.* **34**, 3509.
- [25] Cercignani, C. and Sernagiotto, F. 1966 Cylindrical Poiseuille flow of a rarefied gas. *Phys. Fluids*, **9**, 40.
- [26] Kogan, M. N. 1969 *Rarefied Gas Dynamics*. New York, Plenum Press.
- [27] Bhatnagar, P. L., Gross, E. P. and Krook, M. 1954 A Model for Collision Processes in Gases. I. *Phys. Rev.* **94**, 511.
- [28] Abramowitz, M. 1953 Evaluation of the integral $\int_0^\infty e^{-u^2-x/u} du$. *J. Math. Phys.* **32**, 188.
- [29] Laporte, O. 1937 Absorption coefficients for thermal neutrons. *Phys. Rev.* **52**, 72.
- [30] Welander, P. 1954 On the temperature jump in a rarefied gas. *Arkiv. Fysik* **7**, 507.
- [31] Willis, R. 1962 Comparison of kinetic theory analyses of linearized Couette flow. *Phys. Fluids* **5**, 127.
- [32] Cercignani, C. "Rarefied Gas Dynamics" in *Proceedings of the third symposium on rarefied gas dynamics*, Paris, 1962, edited by Laurmann (Academic Press Inc., New York, 1963)
- [33] Albertoni, S. Cercignani, C. and Gotusso, L. 1963 Numerical evaluation of the slip coefficient. *Phys. Fluids*, **6**, 993.
- [34] Hamaker, H. C. 1937 The London-van der Waals attraction between spherical particles. *Physica IV*, **10**, 1058.
- [35] Abid, S. and Chesters, A., 1994 The drainage and rupture of partially-mobile film between colliding drops at constant velocity approach. *Intl J. Multiphase Flow* **20**, 613.
- [36] Klaseboer, E., Chevaillier, J. Ph., Gourdon, C. and Masbernat, O. 2000 Film drainage between colliding drops at constant approach velocity: experiments and modeling. *J. Coll. Interface Sci.* **229**, 274.